Heterochromatin spreading in cancer cells through HDAC7 mediated histone H3.3 landscape reprogramming.

Ola Hassan[1], Mattia Pizzagalli[1], Laura Jinxuan Wu[1], David Karambizi[1], John P. Zepecki[1], Eduardo Fajardo[2], Andras Fiser[2], Nikos Tapinos[1,3*]

1: Laboratory of Cancer Epigenetics and Plasticity, Brown University, Rhode Island Hospital, Providence, RI, USA

2: Department of Computational and Systems Biology, Albert Einstein College of Medicine, Bronx, NY

3: Department of Neurosurgery, Brown University, Rhode Island Hospital, Providence, RI, USA

*: **Correspondence:**

Nikos Tapinos MD, PhD

Laboratory of Cancer Epigenetics and Plasticity

593 Eddy Street, Providence RI

nikos_tapinos@brown.edu

Abstract

Class IIa histone deacetylases (HDACs) are a family of enzymes that despite their name, do not have any measurable histone deacetylase activity but they function as multi-protein interaction hubs due to the presence of a prolonged N-terminal domain. Here we show that HDAC7, a member of the Class IIa HDAC family, is a chaperone for Histone H3.3 and, interacts with H3.3 and HIRA on chromatin. Specific inhibition of HDAC7 expression with subtype specific siRNAs results in inhibition of the interaction of H3.3 with HIRA, while the association of H3.3 with DAXX and H3K9me3 is significantly increased, resulting in H3.3 being deposited on H3K9me3+/DAPI+ heterochromatin nuclear foci. Inhibition of HDAC7 triggers a significant increase of heterochromatin marks H3K9me3 and H3K27me3, global heterochromatin spreading in cancer cells, and reprogramming of the H3.3 chromatin landscape. This drives substantial alteration of cancer cell gene expression as well as inhibition of the stemness phenotype for cancer cells. Our work demonstrates the involvement of HDAC7 in the euchromatic H3.3 chaperone network and shows that inhibiting HDAC7 induces H3.3 landscape reprogramming, heterochromatin spreading, and epigenetic restriction in cancer cells.

Introduction

Epigenetic mechanisms have emerged as key players in cancer development. Alterations in chromatin mediate cell reprogramming and oncogenesis, while epigenetic changes triggered by the tumor microenvironment regulate cancer cell phenotypic transitions and tumor architecture [1,2]. Chromatin exists in two higher order states: euchromatin refers to loosely packed chromatin that is easily accessible to transcriptional regulators and RNA polymerase, while heterochromatin is densely packed and not accessible [3,4]. Alteration of the state of chromatin impacts global gene expression by making genes either more or less accessible for transcription. Interconversion between these two chromatin states occurs through the function of several regulators that affect levels of DNA methylation or posttranslational modification of histones (acetylation, methylation, phosphorylation, sumoylation etc.). This dynamic regulatory system is commonly referred as the epigenetic control of gene transcription [5].

Histone deacetylases (HDACs) remove acetyl- groups from histone molecules hence regulating posttranslational modification of histone marks. Expression of HDACs is elevated in several tumors resulting in transcriptional activation of oncogenes, increased transcriptional rates and chromosomal translocations [4,6,7]. HDACs can be divided into class I (HDAC1, 2, 3, and 8), class II (HDAC4, 5, 6, 7, 9, and 10), and class IV (HDAC11) based on sequence similarity. The class II HDACs are further divided into class IIa (HDAC4, 5, 7, and 9) and class IIb (HDAC6, and 10), according to their domain compositions. However, Class IIa HDACs lack any measurable enzymatic activity and their deacetylase activity is minimal towards acetylated histones [5]. Class IIa HDACs exhibit a prolonged N-terminal region compared to Class I HDACs that harbors a

nuclear localization signal and a nuclear export signal, so they are found both in the nucleus and the cytoplasm [5]. The presence of this unique N-terminal region suggests that Class IIa HDACs may participate in multi-protein complexes to exert their biological function. In human malignancies, Class I and II HDACs are considered oncoproteins that regulate gene expression to promote tumorigenesis and cancer development [5-7]. Specifically, HDAC7 has been implicated in the pathogenesis of colorectal[8,9], pancreatic[10,11], liver[12], gastric[13], lung[14], breast[15] and brain cancer[16,17].

Canonical histone proteins are incorporated on chromatin in a DNA replication dependent manner, while Histone H3.3 incorporates in a DNA replication independent manner [18-20]. In Drosophila melanogaster and Arabidopsis thaliana, H3.3 is enriched in replication origins [21-26], while in human cells is associated with early replication and recruited on sites of DNA repair [26-28]. Although H3.3 is mainly associated with euchromatin and regulation of active transcription [20,29], recently it was shown that it was also associated with heterochromatin on telomeres, pericentric heterochromatin and heterochromatin marks on gene regulatory regions [29,30]. Association of H3.3 with euchromatin or heterochromatin is largely dependent on a group of proteins with chaperone activity that interact with H3.3 and deposit it on chromatin regions. Euchromatin deposition is regulated by a HIRA/UBN1/CABIN1 chaperone complex while heterochromatin deposition of H3.3 depends on interaction with DAXX/ATRX [31,32]. The balance between HIRA/UBN1/CABIN1 versus DAXX/ATRX deposition of H3.3 on euchromatin or heterochromatin respectively, may represent a crucial node in histone landscape reprogramming that enables complex cell fate decisions during tumorigenesis. Involvement of HDACs on these Histone chaperone complexes has only

been suggested for the MIER1 complex but not for individual HDACs [33] and the participation of Class IIa HDACs in the regulation of the Histone H3.3 chromatin landscape has not been studied to date.

Here we show high expression of HDAC7 in glioblastoma tumors, patients derived glioma stem cells (GSCs), and patient derived pediatric DIPG cells. HDAC7 shows minimal histone deacetylase activity but forms protein-protein interactions with Histone H3.3 on chromatin. Specific inhibition of HDAC7 expression with an in vivo stable siRNA, results in increase of heterochromatin marks H3K9me3 and H3K27me3, global heterochromatin spreading in cancer cells, and rebalancing of the H3.3 chromatin landscape. Following HDAC7 inhibition, the interaction of H3.3 with HIRA is reduced, the association of H3.3 with DAXX and H3K9me3 is significantly increased and H3.3 is deposited on H3K9me3^{+}/DAPI^{+} heterochromatin nuclear foci. This results in significant alteration of cancer cell gene expression, and inhibition of GSC growth and self-renewal. Our work demonstrates the involvement of HDAC7 in euchromatic H3.3 chaperone complexes and shows that inhibition of HDAC7 results in H3.3 landscape reprogramming, heterochromatin spreading and epigenetic restriction in cancer cells.

Results

HDAC7 is highly expressed in glioblastoma tumors and correlates with decreased patient survival.

Using data from The Cancer Genome Atlas (TCGA), we compared the expression of all Class IIa HDACs in glioblastoma. HDAC-7 is the only Class IIa HDAC with significantly higher expression in glioblastoma as compared to the non-tumor samples (Figure 1A). Also, to show clinical correlation of HDAC7 expression in glioblastoma, we performed survival analysis on Class IIa high- and low-expressing patients. Patients were divided into these two groups based

on the maximally ranked statistics using the log rank test as well as Gehan-Breslow-Wilcoxon method. High HDAC7 expressing patients show significantly lower probability of survival ($p<0.004$) (Figure 1B), while the expression level of other members of Class IIa HDACs has no correlation to patient survival.

In collaboration with the Pathology Department at Rhode Island Hospital, we collected 84 PFF tumor samples from patients with confirmed diagnosis of IDH WT Glioblastoma. We performed Nanostring gene expression analysis using the Pan Cancer Panel that contains 770 genes with confirmed roles in cancer. The expression data were clustered based on high versus low expression of HDACs. Classification of gene expression in HDAC7 “high” versus HDAC7 “low” expressing patients, showed that high HDAC7 expression correlates with significant increase in expression of 45 genes and inhibition of 2 genes (Figure 1C). Functional classification of the significantly increased genes shows that they have significant pro-tumorigenic roles like Vimentin, Lox, SERPINH1, TGFb, etc. (Figure 1D). Then we performed Kaplan Meier survival analysis on the 84 patients based on high (n=37) or low expression (n=47) of HDAC7 and showed that patients with high HDAC7 expression had significantly lower disease-free survival (Wilcoxon $p<0.005$) (Figure 1E).

Expression of HDAC7 in cancer cells.

To determine expression levels of HDAC7 in various human cancer cells, we performed Western blotting on lysates from 6 patients derived GSCs with IDH WT glioblastoma and 4 pediatric primary DIPG cells and compared expression to control human astrocytes. We show that HDAC7 is highly expressed in GSCs and DIPG cells while minimally expressed in control human astrocyte lysates (Figure 1F-G).

The presence of nuclear localization and nuclear export signals makes HDAC7 capable of nuclear and cytoplasmic expression depending on the cell type [34,35]. To determine the topology of HDAC7 expression in patients derived GSCs, we performed

immunofluorescent staining of HDAC7 expression (red) and Vimentin (green) as cytoplasmic marker. Nuclei were visualized with DAPI (blue) and z-stack images were acquired with a Zeiss Axiovert inverted microscope equipped with Apotome II. We show that HDAC7 is highly expressed in the nucleus of GSCs with minimal expression in the cytoplasm (Figure 2A).

Class specificity of HDAC7 siRNA.

To determine target specificity of the HDAC7 siRNA, we designed, filtered through BLAST similarity search, and finally synthesized 4 individual siRNAs that target the open reading frame and 3'- untranslated region of human HDAC7. 50nM of each siRNA was separately transfected into patients derived GSCs and the expression of Class IIa HDACs was determined by Western blotting 72 hours after transfection. Control cells were transfected with non-targeting siRNA and Actin was used as loading control. The selected siRNA shows specific inhibition of HDAC7 protein expression and does not affect the expression of HDAC4, HDAC5 and HDAC9 (Figure 2B and Supplementary Figure S1).

MS profiling of histone marks following inhibition of HDAC7 expression.

To determine if HDAC7 has any effect on levels of histone modifications, we performed histone modification Mass Spectrometry (ModSpec-Active Motif) after inhibition of HDAC7 expression with our specific siRNA. Individual histone modifications were quantified by ModSpec and expressed as a proportion of all modified and unmodified residues (% of the peptide pool). At baseline (siControl GSCs), we found histones H3 and H4 to be highly modified. In contrast, H1 and H2 showed minor to no modifications (Figure 2C). The most modified histone sites were H3K9, H3.1K27, H3.3K27 and

H4K20 (Supplementary Figure S2). On aggregate, dimethylation of histone marks shows the highest abundance in comparison to other modifications in GSCs. To determine significant changes in levels of histone modifications following inhibition of HDAC7, we used a cut-off of 3% change and a $P<0.05$. Differences in the total enrichment of all marks (as a proportion of all modified and unmodified peptides) at each of the different histone sites are shown in Figure 2D. We show that inhibition of HDAC7 expression does not affect levels of histone acetylation suggesting minimal histone deacetylase activity but induces significant increase in H3K9me1 and reduction at levels of unmodified H3K9UN, which implies major chromatin landscape restructuring and increase of heterochromatin. In addition, we detect significant increase in H3.3K27me1 and H3.1K27me1, which is a mark that has been associated mainly with heterochromatin [36,37] but also with active transcription in embryonic stem cells [38].

Rapid Immunoprecipitation Mass Spectrometry of Endogenous Proteins (RIME) to identify the HDAC7 interactome on chromatin.

To determine how inhibition of HDAC7 results in increase of heterochromatin marks, we hypothesized that HDAC7 forms multiprotein interactions on euchromatin to participate in regulation of active transcription. We employed Rapid Immunoprecipitation Mass Spectrometry of Endogenous Proteins (RIME) to discover the HDAC7 protein-protein interaction network on chromatin of GSCs. GSCs (n=3) were fixed with formaldehyde to crosslink proteins and DNA that are in very close proximity, nuclei were isolated and HDAC7 immunoprecipitation was performed. The HDAC7 precipitated protein complex was subjected to Mass Spectrometry (RIME) which revealed 247 proteins constituting the HDAC7 interactome. The proteins were entered into STRING for network analysis

using default settings and exported into Cytoscape for network construction. 229 from the 247 proteins formed a highly interconnected network (Figure 3A). To focus the analysis, we extracted the HDAC7 1st degree interactome (Figure 3B). This refers to the complete set of nodes and edges of proteins directly linked to HDAC7 (Figure 3B). There were 10 proteins/genes directly connected with HDAC7, these were NCOR2, H3.3, H3.4, H3C13, H3C12, CTNNB1, CHD4, TBLX1XR1 and HSPA4. The nodes in the resulting network were highly interconnected (PPI p val = 5.28E-18). The HDAC7 1st degree interactome/network was enriched for transcription regulation pathways, notch signaling, chromatin modeling, and Beta-catenin signaling (Figure 3B). Next, we extended the analysis to include nodes connecting directly to the HDAC7 1st degree interactome, thus generating the 1st and 2nd degree interactome (Figure 3C). The 1st and 2nd degree interactome was composed of 84 nodes that were significantly enriched for mitotic activity and cell cycle pathways (Figure 3C).

HDAC7 interacts with Histone H3.3 and the H3.3 mutant variant H3K27M.

To validate the interaction between HDAC7 and H3.3, we performed co-immunoprecipitation (co-IP) experiments using protein lysates from patients derived GSCs (n=3). Immunoprecipitation was performed with an HDAC7 validated antibody (Abcam) and the presence of H3.3 was detected with an H3.3. specific antibody (Active Motif). This showed that HDAC7 co-precipitates with H3.3 (Figure 3A) validating the RIME results. Since the H3.3 mutant variant H3K27M has been implicated in pediatric brain tumors, we performed co-IPs using lysates from patient derived pediatric diffuse pontine glioma (DIPG) cells (kind gift of Dr. Michelle Monje) and showed that HDAC7

interacts and co-precipitates with H3K27M (Figure 3B) suggesting a role for HDAC7 in these pediatric tumors.

Inhibition of HDAC7 reduces interaction of H3.3 with HIRA and increases interaction with DAXX and H3K9me3.

To determine how HDAC7 affects the H3.3. landscape in cancer cells, we inhibited the expression of HDAC7 with siHDAC7 and determined the effects of HDAC7 inhibition on the interaction of H3.3 with its euchromatin chaperone HIRA, or its heterochromatin chaperone DAXX/ATRX. We show that inhibition of HDAC7 results in reduction of the interaction of H3.3 with HIRA in GSCs, increase of the interaction of H3.3 with the heterochromatin chaperone DAXX (Figure 3C), and significant increase in total levels of DAXX (Figure 3D). These results suggest that inhibition of HDAC7 expression results in rebalancing of the H3.3 landscape, reduction of H3.3. association with euchromatin chaperones and increased association of H3.3 with heterochromatin. To verify that inhibition of HDAC7 results in increased association of H3.3 with heterochromatin, we performed co-IP of H3.3 with H3K9me3. This shows that following inhibition of HDAC7 expression, the interaction of H3.3 with heterochromatin mark H3K9me3 is increased significantly (Figure 3E).

HDAC7 inhibition results in increased levels of SETDB1, EZH2, H3K9me3 and H3K27me3.

Since inhibition of HDAC7 results in increased association of H3.3. with heterochromatin, we examined if siHDAC7 induces global increase of heterochromatin marks in cancer cells. We performed Western blot detection of H3K9me3 and H3K27me3 in patients derived GSCs (n=3) and show significant increase of both

H3K9me3 and H3K27me3 (Figure 3F). In addition, protein levels of SETDB1 and EZH2, the histone methyltransferases that mediate the trimethylation of H3K9 and H3K27 respectively, were both significantly elevated following inhibition of HDAC7 (Figure 3F). To verify these results, we performed quantitative ELISA (Active Motif) to detect levels of H3K9me3 and H3K27me3 in 5 patients derived GSCs and show significant increase of both heterochromatin marks following inhibition of HDAC7 (Figure 3G).

Inhibition of HDAC7 induces heterochromatin spreading in cancer cells.

To visualize and quantify the increased association of H3.3 with heterochromatin and the global increase of heterochromatin marks in cancer cell nuclei, we performed immunofluorescence localization of H3.3 and H3K9me3 with and without inhibition of HDAC7 with siRNAs. Quantification of the number of H3.3 containing heterochromatin foci per nucleus from 30 individual cell nuclei shows that siHDAC7 induces a significant increase in localization of H3.3 within heterochromatin foci (Figure 4A-B). In addition, siHDAC7 induces significant increase in H3K9me3 expression in the nucleus of cancer cells (Figure 4C-D). To better visualize the spreading of heterochromatin within the cancer cell nucleus, we performed transmission electron microscopy (TEM) on patient derived GSC nuclei before and after inhibition of HDAC7 with siRNAs. We show that inhibition of HDAC7 results in spreading of electron-dense pericentric heterochromatin and increase of heterochromatin chromobodies (Figure 4F, arrows).

Inhibition of HDAC7 results in broad transcriptomic changes in cancer cells and inhibition of GSC self-renewal.

To assess the effect of HDAC7 inhibition at the transcript expression level, we performed RNA-seq with and without inhibition of HDAC7 expression in GSCs (n=2).

PCA demonstrated appropriate segregation across conditions, suggesting that the siRNA targeting of HDAC7 induced reproducible changes across patients (Figure 6A). We identified 194 downregulated and 432 upregulated genes (adj. p val < 0.001, FC>2) (Figure 6B). Downregulated set of genes showed significant enrichment for cell cycle, synthesis/unwinding of DNA, ATR response to stress (Figure 6C). There was notable decrease in major regulators of cell cycling (CDC6, E2F1, E4F1), genome stability (H2AX, MCM3/5/7) and replication fork progression (ORC1) (Figure 6D). In addition, genes with central role in cancer stem cell biology (Notch, Myc, Raf, JMJD1, etc.) were downregulated following inhibition of HDAC7 expression (Figure 6E). To determine functional significance of the effect of HDAC7 inhibition in transcript expression and since transcripts of major regulators of cell cycle and DNA replication were affected, we performed tumor-sphere formation assay with and without inhibition of HDAC7 in GSCs (n=3). Tumor-sphere formation provides a direct link to cancer stem cell self-renewal and division. We show that inhibition of HDAC7 results in significant inhibition of tumor sphere formation capabilities of human GSCs (p<0.0001) (Figure 6F).

Discussion

Class IIa HDACs have limited catalytic activity in eukaryotic cells mainly due to a substitution of a tyrosine with histidine within the enzymatic pocket of these molecules [39]. Although Class IIa HDACs can bind to acetylated lysine, they don't exert deacetylase activity and it has been proposed that they function to attract other HDAC subtypes to deacetylate the substrates[40,41]. Several studies have shown a role of class IIa HDACs in cancer but the exact function of each member of the class varies depending on the type of cancer[42]. HDAC7 has been implicated in the regulation of cancer stem cell fate,

specifically in breast and ovarian tumors where it was shown that overexpression of HDAC7 can increase the cancer stem cell phenotype [43]. HDAC7 binds near transcription start sites (TSS) and super-enhancers (SEs) of oncogenes in breast cancer stem cells and contributes to their transcriptional regulation. Although it was shown that HDAC7 is required to maintain levels of H3K27Ac at TSS and SEs, how this is achieved has not been determined to date [42,44].

Our findings provide robust evidence supporting the interaction between HDAC7 and Histone H3.3 in glioblastoma stem cells. Through RIME and co-immunoprecipitation, we demonstrated a direct physical association between these molecules. This adds to the growing body of literature elucidating the complex interplay between histone molecules and their regulatory enzymes. The interaction between HDAC7 and Histone H3.3 suggests a potential role for HDAC7 in chromatin remodeling and gene regulation.

The specific interaction with H3.3, a histone variant associated mainly with active chromatin states, underscores the importance of HDAC7 in maintaining chromatin homeostasis. Histone H3.3 is deposited into euchromatin in a DNA replication independent manner. Specifically, H3.3 forms complexes with the histone chaperone HIRA to mediate DNA synthesis independent nucleosome assembly [45]. We show here, that HDAC7 participates in these euchromatin complexes by interacting with H3.3 and HIRA. HDAC7 regulates deposition of H3.3 into euchromatin and inhibition of HDAC7 results in reduction of association of H3.3 with HIRA and increased association of H3.3 with DAXX and H3K9me3. This results in remodeling of the H3.3 landscape in cancer cells resulting in heterochromatin spreading and association of H3.3 with heterochromatin foci. Our study unveils a novel aspect of HDAC7 biology in cancer. The

observed increase in heterochromatin upon HDAC7 inhibition suggests a role for HDAC7 in maintaining the balance between euchromatin and heterochromatin, which is often dysregulated in cancer cells. Dysfunctional chromatin remodeling is a hallmark of cancer, and our findings shed light on the potential contribution of HDAC7 to this process.

The identification of HDAC7 as a regulator of heterochromatin dynamics provides a rationale for exploring inhibition of HDAC7 as potential therapeutic strategy in cancer. By promoting heterochromatin formation, HDAC7 inhibition may suppress oncogenic transcriptional programs and impede tumor progression. This is supported by our RNA-seq data showing significant inhibition of pro-tumorigenic transcription factors and transcripts that promote cancer cell division and DNA replication following loss of HDAC7. In addition, inhibition of HDAC7 results in significant reduction of GSC self-renewal, which is a hallmark of cancer stem cell propagation and growth. Despite the significant findings presented in this study, there are certain limitations that warrant consideration. Although our siRNA is subtype specific and does not affect the expression of other members of the Class IIa HDAC family, delivery of the siRNA in solid tumors as an effective therapeutic in human cancers is challenging. Although, following the mRNA vaccines for COVID, the use of lipid nanoparticles (LNP) for delivery of mRNA payloads has been streamlined, there is still no example of an siRNA therapeutic showing effective pharmacokinetic profile and distribution within solid tumors, suggesting that more research and development efforts need to focus on effective LNP delivery of anti-cancer siRNA therapeutics. In addition, the development of class and subtype specific small molecule inhibitors for HDACs has also been

problematic due to the sequence similarity between subtypes. These limitations are important to overcome to develop an effective anti-HDAC7 therapeutic for human use. Future investigations should aim to address these limitations and further elucidate the molecular mechanisms underlying the role of HDAC7 in chromatin dynamics and cancer pathogenesis. Additionally, exploring the crosstalk between HDAC7 and other chromatin modifiers will deepen our understanding of the regulatory networks governing chromatin organization. A specific HDAC7 interaction that requires further investigation is the reported interaction with HDAC3[46] to determine if specific inhibition of HDAC7 results in alteration of HDAC3 functions in cancer cells.

In summary, our study identifies HDAC7 as a critical regulator of chromatin dynamics and heterochromatin formation in cancer. These findings not only expand our knowledge of HDAC biology but also highlight the therapeutic potential of targeting HDAC7 in cancer treatment. Further research in this area promises to uncover new avenues for precision medicine and improve patient outcomes in oncology.

Materials and Methods

Primary glioblastoma stem cell isolation and culture

The institutional review board (IRB) of Rhode Island Hospital has approved the collection of patient-derived glioblastoma multiforme tissue. All collections were performed with written informed consent from patients in completely de-identified manner and the studies were performed in accordance to recognized ethical guidelines (Belmont Report). Primary GSC spheres were cultured from human glioma samples as previously described[47]. GSCs used in this study were authenticated by ATCC using short tandem repeat analysis. GSCs used were between passages 5 and 30 and

cultured either as spheres or as attached on fibronectin-coated plates (10 mg/mL, Millipore Sigma) in a medium of 1X Neurobasal Medium, B27 serum-free supplement, minus Vitamin A, 100X Glutamax (Fisher Scientific), 1 mg/mL Heparin (STEMCELL Technologies), 20 ng/mL epidermal growth factor (Peprotech), 20 ng/mL bFGF (Peprotech). All GSC cultures are routinely tested for Mycoplasma contamination using the MycoSensor qPCR assay (Agilent).

Analysis of publicly available cancer datasets

For survival analyses, we used the Chinese Glioma Genome Atlas (CGGA) and The Cancer Genome Atlas (TCGA) patient cohorts; patients were assigned to high/low-risk groups based on HDAC7 expression levels. The datasets were downloaded from GlioVis and visualized in the Kaplan-Meier Plotter[48], GlioVis[49] web tools, and via the R Bioconductor package.

Nanostring PanCancer progression analysis

We collected RNA from 84 paraffin-embedded samples from glioblastoma patients and performed gene expression analysis using the Nanostring PanCancer progression panel that comprises the vital components of pathways involved in the complex interplay between the tumor and its microenvironment. Overall survival was estimated by the Kaplan-Meier method at GraphPad prism. Pathway enrichment and Gene ontology enrichment analyses were performed on the differentially expressed genes using R package DESeq[50].

siRNA transfection

GSCs were grown over fibronectin/HBSS-treated culture plates in antibiotic-free media supplemented with Neurobasal-A, B-27-A, Glutamax, growth factors (EGF and FGF),

and heparin, and GSCs were incubated at 37°C with 5 % CO2 overnight. 50nM of HDAC7 siRNAs was used for all experiments. The sequences of the 4 HDAC7 siRNAs used in this study and the control non targeting siRNA are:

siRNA-1 sense: 5' G.A.C.A.A.G.A.G.C.A.A.G.C.G.A.A.G.U.G 3'

antisense: 5' C.A.C.U.U.C.G.C.U.U.G.C.U.C.U.U.G.U.C 3'

siRNA-2 sense: 5' G.C.A.G.A.U.A.C.C.C.U.C.G.G.C.U.G.A.A 3'

antisense: 5' U.U.C.A.G.C.C.G.A.G.G.G.U.A.U.C.U.G.C 3'

siRNA-3 sense: 5' G.G.U.G.A.G.G.G.C.U.U.C.A.A.U.G.U.C.A 3'

antisense: 5' U.G.A.C.A.U.U.G.A.A.G.C.C.C.U.C.A.C.C 3'

siRNA-4 sense: 5' U.G.G.C.U.G.C.U.U.C.U.C.G.G.G.U.U.A.A 3'

antisense: 5' U.U.A.A.C.C.C.G.A.G.A.A.G.C.A.G.C.C.A 3'

Non-targeting control siRNA- sense: 5' A.G.C.G.A.C.U.A.A.A.C.A.C.A.U.C.A.A 3'

antisense: 5' U.U.G.A.U.G.U.G.U.U.U.A.G.U.C.G.C.U 3'

Tumor sphere formation assay

Tumor sphere formation assay was performed as described before[51]. Sphere formation by visual counting was estimated after seven days in a blinded, unbiased format by counting the number of spheres in each well by two independent researchers.

RNA Sequencing

Next-generation RNA-sequencing was performed using an Illumina HiSeq2500 system (Azenta). Sequence reads were aligned to the human genome using *gsnap*. Genomic locations of genes and exons were extracted from the *refGene.txt* file (http://hgdownload.cse.ucsc. edu/goldenPath/hg38/database/refGene.txt.gz). Fo analysis, we used a false discovery rate FDR<0.001.

Mass Spectrometry for Histone Modifications (Mod-Spec)

Five million GSCs were harvested, washed twice with PBS and snap frozen. Successful knock-down of HDAC7 was confirmed by Western blot and the samples were sent to Active Motif to perform Mod Spec per their in-house protocols. The entire Mass Spec process was repeated three separate times for each sample. The data was quantified using Skyline[52] and presented as the percent of each modification within the total pool of that tryptic peptide.

Rapid-immunoprecipitation-mass-spectrometry-of-endogenous-protein (RIME)

Two biological replicates of GSCs (5 x 10^8 cells per replicate) were fixed for 8 minutes with a formaldehyde solution of 11% Methanol Free Formaldehyde, 0.1M NaCl (Invitrogen™), 1 mM EDTA, pH 8 (Invitrogen™), and 50mM HEPES, pH 7.9 (Fisher BioReagents™). Fixation was stopped using 2.5 M Glycine solution in water (Sigma). Fixed cells were washed with chilled PBS-Igepal (0.5% Igepal CA-630 in PBS) and PMSF (Active Motif). Washed cells were centrifuged, pelleted, and snap-frozen on dry ice and sent to Active Motif for RIME® service[53]. PEAKS Studio was used for visualization and analysis, and the “Decoy Fused Method” was applied for calculating FDR where the default cutoff is set to -10logP > 20 to ensure high-quality peptide spectrum matches and increase confidence in the proteins list obtained.

Co-immunoprecipitation followed by western blot

After the respective course of treatment, GSCs (10 million cells / Co-IP) were collected and prepared for nuclear extraction and purification using a nuclear extraction kit (Active Motif). Nuclear extracts were treated with an enzymatic shearing Cocktail for DNA digestion to release undissociated protein complexes, including histone proteins and

DNA-binding proteins from the DNA. 500 µg of extracted and purified nuclear lysate was used per IP per after pre-clearing with normal IgG (same concentration as the respective IP antibody) for 1 hour on a rotator at 4°C. Pre-cleared nuclear lysates were then combined with 25 µl of Protein G beads and incubated for 1 hour on a rotator at 4°C to clear away any IgG nonspecific binding. After separating the magnetic beads on a magnetic stand, the collected nuclear supernatant was then combined with the IP antibodies of either 1 µg HDAC7 (Cell Signaling) or 4 µg H3.3 (Abcam) and incubated for 4 hours on a rotator at 4°C. The immunoprecipitated samples were then combined with 25 µl of Protein G beads and incubated for 1 hour on a rotator at 4°C. After separating the magnetic beads on a magnetic stand, the immunoprecipitated samples (now bound to the beads) were washed four times with Co-IP wash buffer (Active Motif). The washed immunoprecipitated samples bound to beads were then resuspended in 20 µl of 2X Reducing Loading Buffer (130 mM Tris pH 6.8, 4% SDS, 0.02% Bromophenol blue, 20% glycerol, 100 mM DTT) and boiled at 95°C for 5 minutes. Magnetic beads were then separated from desaturated samples using a magnetic stand. All extraction and IP steps were performed in buffers supplemented with Protease and Phosphatase and Inhibitors to limit further protein modifications (expression, proteolysis, dephosphorylation, etc.). Immunoprecipitated samples were analyzed by Western blot.

Histone lysates extraction and purification

The histone acid precipitation technique was used to extract pure crude histones from GSCs following the transfection treatment. After the course of treatment, GSCs were detached using StemPro Accutase (Gibco), and spun-down pellets were collected. Pellets were then resuspended in the appropriate volume of ice-cold histone extraction

buffer (Active Motif) and incubated overnight at 4°C on a rotator. On the next day, cell suspensions were centrifuged to collect core histone extracts. Acid extractions were pH measured and neutralized with the needed volume of 5X neutralization buffer until it reached complete neutralization. Core histones were then purified with column elution, and purified histone lysates were stored at -80°C for downstream experiments.

H3K9Me3 and H3K27Me3 ELISA

Purified core histone extracts prepared as described above were quantified for histone lysine trimethylation at lysine 9 and lysine 27 following ELISA protocols from Active motif (Catalogue # 53109 and 53106, respectively). Absorbance at 450nm with a reference wavelength of 655 nm was read on Promega™ GloMax® Plate Reader. Absorbance was normalized after subtracting blank wells. The quantification for methyl Lys9 and methyl Lys27 from histone H3 in the samples in both assays was obtained using a standard curve plotted in GraphPad prism.

Electron microscopy (EM)

Treated GSCs were harvested, and pellets were resuspended in a 5 ml volume of fixative master mix of Paraformaldehyde-Glutaraldehyde Solution Karnovsky's Fixative (Electron Microscopy Sciences). Fixative solution was prepared with 16% paraformaldehyde solution, 5% Glutaraldehyde EM Grade, and 0.2 M Sodium phosphate buffer. Fixed samples were outsourced to Charles River laboratories for EM imaging service (Frederick PAI Project No. 20354508). Each sample was examined on a transmission electron microscope (TEM), and up to 10 representative digital images per sample were taken with an AMT camera.

Immunofluorescence

Primary glioblastoma stem cells were seeded in complete media without heparin on cell-culture treated chamber slides (Ibidi) overnight and transfected after 24 hours with x2 lipid (Mirus Bio) and either 25 nM control (Horizon) or HDAC7 (Horizon) siRNA. All immunofluorescence staining was performed 48 hours post-transfection.

For H3.3, cells were fixed/permeabilized with 100% ice-cold methanol for 5 min and incubated in blocking buffer (1% BSA, 10% donkey serum, 22.52 mg/mL glycine in PBST (PBS+ 0.1% Tween 20)) for 1 hour at room temperature. Primary antibody (Abcam) was applied 1:1000 in primary antibody buffer (1% BSA in PBST) overnight at 4°C. Cells were washed with DPBS and incubated with secondary antibody (Jackson) 1:100 in DPBS for 1 hour and mounted with DAPI (Vector Labs).

For H3k9me3, cells were fixed with 4% paraformaldehyde (methanol-free) for 10 min, permeabilized with .1% Triton in DPBS for 5 min. Blocking, primary antibody (Active Motif), secondary antibody, and mounting was applied as described above.

Images were taken using a Zeiss Axiovert Inverted Microscope with Apotome II.

QUANTIFICATION AND STATISTICAL ANALYSIS

To determine significance among the means of two independent groups, we perform an unpaired two-tailed t test. To verify Gaussian distribution of data before applying the t test, we perform the D'Agostino and Pearson and Shapiro-Wilk normality tests.

To calculate sample size, we assume the following:

Input: Tails= two**,** Effect size Delta= 2.5**,** α error probe= 0.05**,** Power (1-β err probe)= 0.90**,** Allocation ration N2/N1= 1

Output: Noncentrality parameter δ= 3.9528471**,** Critical t= 2.3**,** Df=8

Actual Power= 0.9

Significance is stated as follows: (ns), $p < 0.05$ (*), $p < 0.01$ (**), $p < 0.001$ (***), $p < 0.0001$ (****).

RESOURCE AVAILABILITY

Further information and requests for resources and reagents should be directed to and will be fulfilled by the lead contact, Nikos Tapinos (nikos_tapinos@brown.edu).

Acknowledgments

The authors would like to thank the Department of Pathology at Rhode Island Hospital for providing the glioblastoma tissue samples for Nanostring Analysis. We also thank Charles River for Electron Microscopy services. This study was supported by a Warren Alpert Foundation Grant #17775 to N.T., private philanthropic donations to the Laboratory of Cancer Epigenetics and Plasticity and from internal support of the Neurosurgery Department of Brown University to N.T.

Conflict of Interest Disclosure

The authors declare no conflict of interest.

References

1. Wainwright, E.N., and Scaffidi, P. (2017). Epigenetics and Cancer Stem Cells: Unleashing, Hijacking, and Restricting Cellular Plasticity. Trends Cancer *3*, 372-386. 10.1016/j.trecan.2017.04.004.
2. Guetta-Terrier, C., Karambizi, D., Akosman, B., Zepecki, J.P., Chen, J.S., Kamle, S., Fajardo, J.E., Fiser, A., Singh, R., Toms, S.A., et al. (2023). Chi3l1 Is a Modulator of Glioma Stem Cell States and a Therapeutic Target in Glioblastoma. Cancer Res *83*, 1984-1999. 10.1158/0008-5472.CAN-21-3629.
3. Allfrey, V.G., Faulkner, R., and Mirsky, A.E. (1964). Acetylation and Methylation of Histones and Their Possible Role in the Regulation of Rna Synthesis. Proc Natl Acad Sci U S A *51*, 786-794. 10.1073/pnas.51.5.786.
4. Li, G., Tian, Y., and Zhu, W.G. (2020). The Roles of Histone Deacetylases and Their Inhibitors in Cancer Therapy. Front Cell Dev Biol *8*, 576946. 10.3389/fcell.2020.576946.
5. Park, S.Y., and Kim, J.S. (2020). A short guide to histone deacetylases including recent progress on class II enzymes. Exp Mol Med *52*, 204-212. 10.1038/s12276-020-0382-4.

6. Falkenberg, K.J., and Johnstone, R.W. (2014). Histone deacetylases and their inhibitors in cancer, neurological diseases and immune disorders. Nat Rev Drug Discov *13*, 673-691. 10.1038/nrd4360.
7. West, A.C., and Johnstone, R.W. (2014). New and emerging HDAC inhibitors for cancer treatment. J Clin Invest *124*, 30-39. 10.1172/JCI69738.
8. Stypula-Cyrus, Y., Damania, D., Kunte, D.P., Cruz, M.D., Subramanian, H., Roy, H.K., and Backman, V. (2013). HDAC up-regulation in early colon field carcinogenesis is involved in cell tumorigenicity through regulation of chromatin structure. PLoS One *8*, e64600. 10.1371/journal.pone.0064600.
9. Gao, S., Liu, H., Hou, S., Wu, L., Yang, Z., Shen, J., Zhou, L., Zheng, S.S., and Jiang, B. (2018). MiR-489 suppresses tumor growth and invasion by targeting HDAC7 in colorectal cancer. Clin Transl Oncol *20*, 703-712. 10.1007/s12094-017-1770-7.
10. Ouaissi, M., Sielezneff, I., Silvestre, R., Sastre, B., Bernard, J.P., Lafontaine, J.S., Payan, M.J., Dahan, L., Pirro, N., Seitz, J.F., et al. (2008). High histone deacetylase 7 (HDAC7) expression is significantly associated with adenocarcinomas of the pancreas. Ann Surg Oncol *15*, 2318-2328. 10.1245/s10434-008-9940-z.
11. Ouaissi, M., Silvy, F., Loncle, C., Ferraz da Silva, D., Martins Abreu, C., Martinez, E., Berthezene, P., Cadra, S., Le Treut, Y.P., Hardwigsen, J., et al. (2014). Further characterization of HDAC and SIRT gene expression patterns in pancreatic cancer and their relation to disease outcome. PLoS One *9*, e108520. 10.1371/journal.pone.0108520.
12. Freese, K., Seitz, T., Dietrich, P., Lee, S.M.L., Thasler, W.E., Bosserhoff, A., and Hellerbrand, C. (2019). Histone Deacetylase Expressions in Hepatocellular Carcinoma and Functional Effects of Histone Deacetylase Inhibitors on Liver Cancer Cells In Vitro. Cancers (Basel) *11*. 10.3390/cancers11101587.
13. Yu, Y., Cao, F., Yu, X., Zhou, P., Di, Q., Lei, J., Tai, Y., Wu, H., Li, X., Wang, X., et al. (2017). The expression of HDAC7 in cancerous gastric tissues is positively associated with distant metastasis and poor patient prognosis. Clin Transl Oncol *19*, 1045-1054. 10.1007/s12094-017-1639-9.
14. Wei, Y., Zhou, F., Zhou, H., Huang, J., Yu, D., and Wu, G. (2018). Endothelial progenitor cells contribute to neovascularization of non-small cell lung cancer via histone deacetylase 7-mediated cytoskeleton regulation and angiogenic genes transcription. Int J Cancer *143*, 657-667. 10.1002/ijc.31349.
15. Wu, M.Y., Fu, J., Xiao, X., Wu, J., and Wu, R.C. (2014). MiR-34a regulates therapy resistance by targeting HDAC1 and HDAC7 in breast cancer. Cancer Lett *354*, 311-319. 10.1016/j.canlet.2014.08.031.
16. Yu, X., Wang, M., Wu, J., Han, Q., and Zhang, X. (2019). ZNF326 promotes malignant phenotype of glioma by up-regulating HDAC7 expression and activating Wnt pathway. J Exp Clin Cancer Res *38*, 40. 10.1186/s13046-019-1031-4.
17. Peixoto, P., Blomme, A., Costanza, B., Ronca, R., Rezzola, S., Palacios, A.P., Schoysman, L., Boutry, S., Goffart, N., Peulen, O., et al. (2016). HDAC7 inhibition resets STAT3 tumorigenic activity in human glioblastoma independently of EGFR and PTEN: new opportunities for selected targeted therapies. Oncogene *35*, 4481-4494. 10.1038/onc.2015.506.

18. Ahmad, K., and Henikoff, S. (2002). The histone variant H3.3 marks active chromatin by replication-independent nucleosome assembly. Mol Cell *9*, 1191-1200. 10.1016/s1097-2765(02)00542-7.
19. Schwartz, B.E., and Ahmad, K. (2005). Transcriptional activation triggers deposition and removal of the histone variant H3.3. Genes Dev *19*, 804-814. 10.1101/gad.1259805.
20. Szenker, E., Ray-Gallet, D., and Almouzni, G. (2011). The double face of the histone variant H3.3. Cell Res *21*, 421-434. 10.1038/cr.2011.14.
21. Deal, R.B., Henikoff, J.G., and Henikoff, S. (2010). Genome-wide kinetics of nucleosome turnover determined by metabolic labeling of histones. Science *328*, 1161-1164. 10.1126/science.1186777.
22. MacAlpine, H.K., Gordan, R., Powell, S.K., Hartemink, A.J., and MacAlpine, D.M. (2010). Drosophila ORC localizes to open chromatin and marks sites of cohesin complex loading. Genome Res *20*, 201-211. 10.1101/gr.097873.109.
23. Eaton, M.L., Prinz, J.A., MacAlpine, H.K., Tretyakov, G., Kharchenko, P.V., and MacAlpine, D.M. (2011). Chromatin signatures of the Drosophila replication program. Genome Res *21*, 164-174. 10.1101/gr.116038.110.
24. Stroud, H., Otero, S., Desvoyes, B., Ramirez-Parra, E., Jacobsen, S.E., and Gutierrez, C. (2012). Genome-wide analysis of histone H3.1 and H3.3 variants in Arabidopsis thaliana. Proc Natl Acad Sci U S A *109*, 5370-5375. 10.1073/pnas.1203145109.
25. Paranjape, N.P., and Calvi, B.R. (2016). The Histone Variant H3.3 Is Enriched at Drosophila Amplicon Origins but Does Not Mark Them for Activation. G3 (Bethesda) *6*, 1661-1671. 10.1534/g3.116.028068.
26. Strobino, M., Wenda, J.M., Padayachy, L., and Steiner, F.A. (2020). Loss of histone H3.3 results in DNA replication defects and altered origin dynamics in C. elegans. Genome Res *30*, 1740-1751. 10.1101/gr.260794.120.
27. Adam, S., Polo, S.E., and Almouzni, G. (2013). Transcription recovery after DNA damage requires chromatin priming by the H3.3 histone chaperone HIRA. Cell *155*, 94-106. 10.1016/j.cell.2013.08.029.
28. Clement, C., Orsi, G.A., Gatto, A., Boyarchuk, E., Forest, A., Hajj, B., Mine-Hattab, J., Garnier, M., Gurard-Levin, Z.A., Quivy, J.P., and Almouzni, G. (2018). High-resolution visualization of H3 variants during replication reveals their controlled recycling. Nat Commun *9*, 3181. 10.1038/s41467-018-05697-1.
29. Shi, L., Wen, H., and Shi, X. (2017). The Histone Variant H3.3 in Transcriptional Regulation and Human Disease. J Mol Biol *429*, 1934-1945. 10.1016/j.jmb.2016.11.019.
30. Goldberg, A.D., Banaszynski, L.A., Noh, K.M., Lewis, P.W., Elsaesser, S.J., Stadler, S., Dewell, S., Law, M., Guo, X., Li, X., et al. (2010). Distinct factors control histone variant H3.3 localization at specific genomic regions. Cell *140*, 678-691. 10.1016/j.cell.2010.01.003.
31. Drane, P., Ouararhni, K., Depaux, A., Shuaib, M., and Hamiche, A. (2010). The death-associated protein DAXX is a novel histone chaperone involved in the replication-independent deposition of H3.3. Genes Dev *24*, 1253-1265. 10.1101/gad.566910.
32. Lewis, P.W., Elsaesser, S.J., Noh, K.M., Stadler, S.C., and Allis, C.D. (2010). Daxx is an H3.3-specific histone chaperone and cooperates with ATRX in replication-independent

chromatin assembly at telomeres. Proc Natl Acad Sci U S A *107*, 14075-14080. 10.1073/pnas.1008850107.
33. Wang, S., Fairall, L., Pham, T.K., Ragan, T.J., Vashi, D., Collins, M.O., Dominguez, C., and Schwabe, J.W.R. (2023). A potential histone-chaperone activity for the MIER1 histone deacetylase complex. Nucleic Acids Res *51*, 6006-6019. 10.1093/nar/gkad294.
34. Martin, M., Kettmann, R., and Dequiedt, F. (2007). Class IIa histone deacetylases: regulating the regulators. Oncogene *26*, 5450-5467. 10.1038/sj.onc.1210613.
35. Kao, H.Y., Verdel, A., Tsai, C.C., Simon, C., Juguilon, H., and Khochbin, S. (2001). Mechanism for nucleocytoplasmic shuttling of histone deacetylase 7. J Biol Chem *276*, 47496-47507. 10.1074/jbc.M107631200.
36. Loyola, A., Tagami, H., Bonaldi, T., Roche, D., Quivy, J.P., Imhof, A., Nakatani, Y., Dent, S.Y., and Almouzni, G. (2009). The HP1alpha-CAF1-SetDB1-containing complex provides H3K9me1 for Suv39-mediated K9me3 in pericentric heterochromatin. EMBO Rep *10*, 769-775. 10.1038/embor.2009.90.
37. Dong, J., LeBlanc, C., Poulet, A., Mermaz, B., Villarino, G., Webb, K.M., Joly, V., Mendez, J., Voigt, P., and Jacob, Y. (2021). H3.1K27me1 maintains transcriptional silencing and genome stability by preventing GCN5-mediated histone acetylation. Plant Cell *33*, 961-979. 10.1093/plcell/koaa027.
38. Ferrari, K.J., Scelfo, A., Jammula, S., Cuomo, A., Barozzi, I., Stutzer, A., Fischle, W., Bonaldi, T., and Pasini, D. (2014). Polycomb-dependent H3K27me1 and H3K27me2 regulate active transcription and enhancer fidelity. Mol Cell *53*, 49-62. 10.1016/j.molcel.2013.10.030.
39. Lahm, A., Paolini, C., Pallaoro, M., Nardi, M.C., Jones, P., Neddermann, P., Sambucini, S., Bottomley, M.J., Lo Surdo, P., Carfi, A., et al. (2007). Unraveling the hidden catalytic activity of vertebrate class IIa histone deacetylases. Proc Natl Acad Sci U S A *104*, 17335-17340. 10.1073/pnas.0706487104.
40. Brancolini, C., Di Giorgio, E., Formisano, L., and Gagliano, T. (2021). Quis Custodiet Ipsos Custodes (Who Controls the Controllers)? Two Decades of Studies on HDAC9. Life (Basel) *11*. 10.3390/life11020090.
41. Di Giorgio, E., and Brancolini, C. (2016). Regulation of class IIa HDAC activities: it is not only matter of subcellular localization. Epigenomics *8*, 251-269. 10.2217/epi.15.106.
42. Brancolini, C., Gagliano, T., and Minisini, M. (2022). HDACs and the epigenetic plasticity of cancer cells: Target the complexity. Pharmacol Ther *238*, 108190. 10.1016/j.pharmthera.2022.108190.
43. Witt, A.E., Lee, C.W., Lee, T.I., Azzam, D.J., Wang, B., Caslini, C., Petrocca, F., Grosso, J., Jones, M., Cohick, E.B., et al. (2017). Identification of a cancer stem cell-specific function for the histone deacetylases, HDAC1 and HDAC7, in breast and ovarian cancer. Oncogene *36*, 1707-1720. 10.1038/onc.2016.337.
44. Caslini, C., Hong, S., Ban, Y.J., Chen, X.S., and Ince, T.A. (2019). HDAC7 regulates histone 3 lysine 27 acetylation and transcriptional activity at super-enhancer-associated genes in breast cancer stem cells. Oncogene *38*, 6599-6614. 10.1038/s41388-019-0897-0.
45. Tagami, H., Ray-Gallet, D., Almouzni, G., and Nakatani, Y. (2004). Histone H3.1 and H3.3 complexes mediate nucleosome assembly pathways dependent or independent of DNA synthesis. Cell *116*, 51-61. 10.1016/s0092-8674(03)01064-x.

46. Fischle, W., Dequiedt, F., Fillion, M., Hendzel, M.J., Voelter, W., and Verdin, E. (2001). Human HDAC7 histone deacetylase activity is associated with HDAC3 in vivo. J Biol Chem *276*, 35826-35835. 10.1074/jbc.M104935200.
47. Zepecki, J.P., Snyder, K.M., Moreno, M.M., Fajardo, E., Fiser, A., Ness, J., Sarkar, A., Toms, S.A., and Tapinos, N. (2018). Regulation of human glioma cell migration, tumor growth, and stemness gene expression using a Lck targeted inhibitor. Oncogene. 10.1038/s41388-018-0546-z.
48. Menyhart, O., Nagy, A., and Gyorffy, B. (2018). Determining consistent prognostic biomarkers of overall survival and vascular invasion in hepatocellular carcinoma. R Soc Open Sci *5*, 181006. 10.1098/rsos.181006.
49. Bowman, R.L., Wang, Q., Carro, A., Verhaak, R.G., and Squatrito, M. (2017). GlioVis data portal for visualization and analysis of brain tumor expression datasets. Neuro Oncol *19*, 139-141. 10.1093/neuonc/now247.
50. Love, M.I., Huber, W., and Anders, S. (2014). Moderated estimation of fold change and dispersion for RNA-seq data with DESeq2. Genome Biol *15*, 550. 10.1186/s13059-014-0550-8.
51. Johnson, S., Chen, H., and Lo, P.K. (2013). In vitro Tumorsphere Formation Assays. Bio Protoc *3*. 10.21769/bioprotoc.325.
52. MacLean, B., Tomazela, D.M., Shulman, N., Chambers, M., Finney, G.L., Frewen, B., Kern, R., Tabb, D.L., Liebler, D.C., and MacCoss, M.J. (2010). Skyline: an open source document editor for creating and analyzing targeted proteomics experiments. Bioinformatics *26*, 966-968. 10.1093/bioinformatics/btq054.
53. Mohammed, H., Taylor, C., Brown, G.D., Papachristou, E.K., Carroll, J.S., and D'Santos, C.S. (2016). Rapid immunoprecipitation mass spectrometry of endogenous proteins (RIME) for analysis of chromatin complexes. Nat Protoc *11*, 316-326. 10.1038/nprot.2016.020.

Figure Legends

Figure 1: HDAC7 is highly expressed in glioblastoma tissue, GSCs and DIPG cells and correlates with significant decrease in patient survival. A) Transcript expression of Class IIa HDACs in glioblastoma compared to non-tumor control tissue using TCGA data. HDAC7 is the only Class IIa HDAC that is expressed significantly higher in glioblastoma compared to control tissue. B) Kaplan Meier survival analysis from the TCGA data, shows that high expression of HDAC7 is significantly ($p<0.003$) correlated with decreased patient survival. C) Clustering of transcript expression in 84 tissue samples from glioblastoma patients based on high versus low expression of

HDAC7 reveals high expression of 45 transcripts (log2FC>0.5) in patient tumors that express high HDAC7. D) Functional classification of the significantly increased genes shows that they have significant pro-tumorigenic roles like Vimentin, Lox, SERPINH1, TGFb. E) Kaplan Meier survival analysis in 84 patients with glioblastoma from Rhode Island Hospital reveals that high expression of HDAC7 correlates with significant decrease in survival probability ($p<0.005$). F) Expression of HDAC7 in 6 patients derived GSCs as detected by Western blot. G) Expression of HDAC7 in 3 patients derived pediatric DIPG cells compared to normal human astrocytes.

Figure 2: HDAC7 specific knock-down does not alter histone acetylation status but increases heterochromatin marks in GSCs. A) Nuclear expression of HDAC7 in patient derived GSCs stained with an HDAC7 antibody (magenta) and vimentin (green) as a cytoplasmic marker. No-primary antibody control shows lack of non-specific staining. B) Class specificity of the HDAC7 in vivo stable siRNA. siHDAC7 induces significant knockdown of HDAC7 protein expression ($p<0.0001$, n=5) whole is does not affect the expression of the other members of the Class IIa HDAC family (n=3, n.s.). C) Circular plot shows percent abundance of histone modifications in GSCs. Asterisks are used to indicate histone sites undergoing significant alterations following HDAC7 knock down. D) Volcano plot of differentially modified histone marks in control versus siHDAC7 samples (cut-off of 3% change and $P<0.05$).

Figure 3: HDAC7 interactome on chromatin of patient derived GSCs. A) Network of 229 nodes derived from RIME identified proteins interacting with HDAC7 (1E-16). HDAC7 is shown near the center of the network. B) 1st degree interactome: the proteins directly interacting with HDAC7. Each protein/gene is color-coded based on functional

enrichment. Corresponding enrichment analysis shown. 3C) 1st & 2nd degree interactome: Proteins connected to those directly interacting to HDAC7. Corresponding enrichment analysis shown.

Figure 4: HDAC7 interacts with H3.3 and HIRA and inhibition of HDAC7 increases DAXX and deposits H3.3 on H3K9me3 and H3K27me3 heterochromatin. A) HDAC7 and Histone H3.3 co-immunoprecipitation from nuclear lysates of GSCs. Representative example of 3 independent experiments. B) HDAC7 and oncohistone H3.3K27M co-immunoprecipitation from nuclear lysates of pediatric DIPG cells. C) Inhibition of HDAC7 results in loss of H3.3 interaction with HIRA and increase in interaction of H3.3 with DAXX. Co-immunoprecipitations were repeated 3 independent times. D) Inhibition of HDAc7 results in significant increase of DAXX in the nucleus of GSCs ($p<0.05$, n=3). E) HDAC7 knockdown results in significant increase in the direct association of histone H3.3 with the heterochromatin mark H3K9me3 ($p<0.05$, n=3). F) Inhibition of HDAC7 expression in GSCs results in significant increase in levels of SETDB1, EZH2, H3K9me3 and H3K27me3 ($p<0.05$, n=3, n=4). G) H3K9me3 and H3K27me3 ELISA on nuclear lysates from three independent patients derived GSCs shows significant increase of both heterochromatin marks (*$p<0.05$, **$p<0.01$, n=3, n=4).

Figure 5: Inhibition of HDAC7 results in H3.3 landscape rebalancing and heterochromatin spreading in cancer cells. A) Immunofluorescence staining of H3.3 (red) and DAPI (blue) in GSCs before and after knock-down of HDAC7 shows that inhibition of HDAC7 expression results in redistribution of H3.3 from $DAPI^{(-)}$ euchromatin nuclear domains to $DAPI^{(+)}$ heterochromatin foci. B) Quantification of the number of

H3.3+ heterochromatin foci per nucleus from 30 GSC nuclei per condition (siControl vs siHDAC7). There is a significant increase in the average number of H3.3+ heterochromatin foci following HDAC7 inhibition. Control average number of H3.3+ foci: 3.14 +/- 2.5, siHDAC7 average number of H3.3+ heterochromatin foci: 7 +/- 3.5. P<1.3E-05. C) Immunofluorescence staining of H3K9me3 (red) and DAPI (blue) in GSCs before and after knock-down of HDAC7 shows that inhibition of HDAC7 expression results in increase of the heterochromatin mark in the nucleus of GSCs. D) Quantification of the number of H3K9me3+ foci in the nucleus of 20 GSCs with and without inhibition of HDAC7 shows significant increase in the number of H3K9me3+ foci following inhibition of HDAC7 (p<3.2E-05). E) Transmission electron microscopy of patient derived GSCs before (siControl) and after (siHDAC7) inhibition of HDAC7 expression shows spreading of electron dense heterochromatin in pericentric nuclear domains (arrowhead) and nuclear chromobodies (arrows).

Figure 6: Transcript expression analysis and tumor sphere formation assay in GSCs following inhibition of HDAC7 expression. A) PCA plot of GSCs in control versus siHDAC7 samples. B) Volcano plot of differentially expressed genes following HDAC7 knock down (adj. p val < 0.001, FC>2). C) Pathway enrichment of downregulated genes. D) Heat Map showing decrease in major regulators of cell cycling (CDC6, E2F1, E4F1), genome stability (H2AX, MCM3/5/7) and replication fork progression (ORC1). E) Heat Map showing significant downregulation of genes with central role in cancer stem cell biology following inhibition of HDAC7 expression.
F) Tumor sphere formation assay shows significant (p<0.0001) inhibition of GSC self-renewal following inhibition of HDAC7 expression.

Figure 1

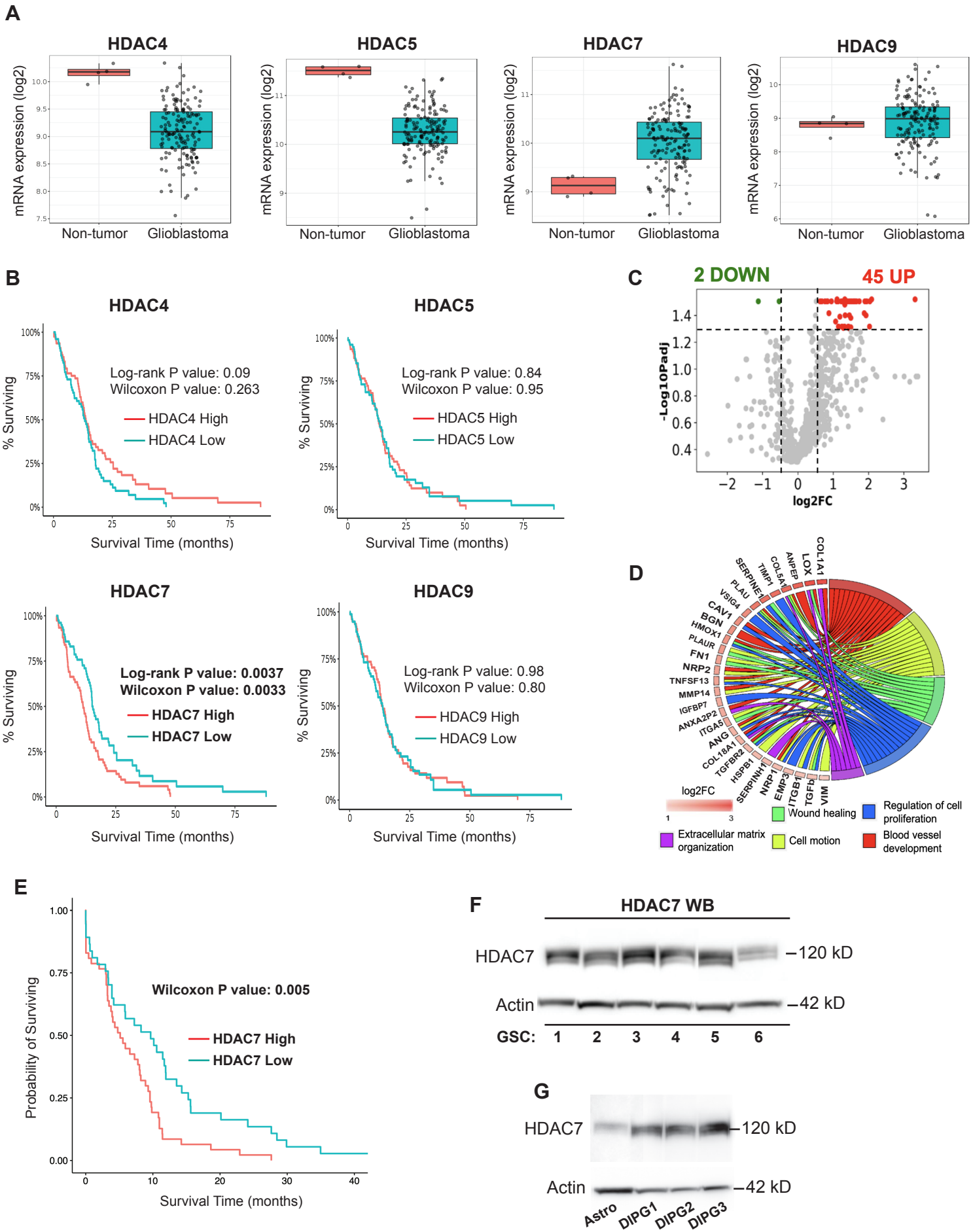
A
HDAC4
HDAC5
HDAC7
HDAC9
mRNA expression (log2)
Non-tumor
Glioblastoma
B
HDAC4
Log-rank P value: 0.09
Wilcoxon P value: 0.263
HDAC4 High
HDAC4 Low
HDAC5
Log-rank P value: 0.84
Wilcoxon P value: 0.95
HDAC5 High
HDAC5 Low
HDAC7
Log-rank P value: 0.0037
Wilcoxon P value: 0.0033
HDAC7 High
HDAC7 Low
HDAC9
Log-rank P value: 0.98
Wilcoxon P value: 0.80
HDAC9 High
HDAC9 Low
% Surviving
Survival Time (months)
C
2 DOWN
45 UP
-Log10Padj
log2FC
D
log2FC
Wound healing
Regulation of cell proliferation
Extracellular matrix organization
Cell motion
Blood vessel development
E
Wilcoxon P value: 0.005
HDAC7 High
HDAC7 Low
Probability of Surviving
Survival Time (months)
F
HDAC7 WB
HDAC7
Actin
120 kD
42 kD
GSC: 1 2 3 4 5 6
G
HDAC7
Actin
120 kD
42 kD
Astro
DIPG1
DIPG2
DIPG3

Figure 2

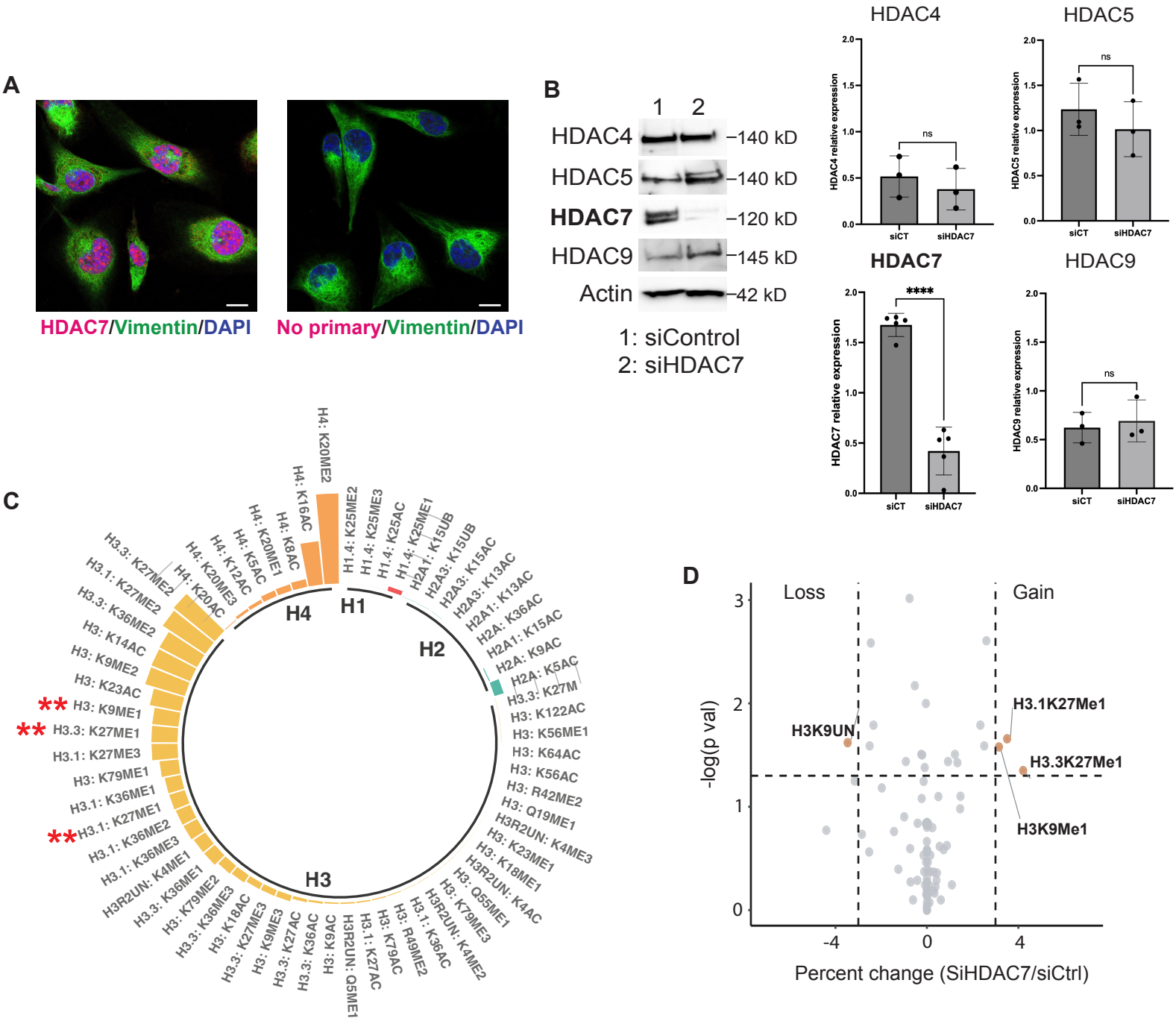
A
HDAC7/Vimentin/DAPI
No primary/Vimentin/DAPI
B
1 2
HDAC4 140 kD
HDAC5 140 kD
HDAC7 120 kD
HDAC9 145 kD
Actin 42 kD
1: siControl
2: siHDAC7
HDAC4
HDAC5
HDAC7
HDAC9
HDAC4 relative expression
HDAC5 relative expression
HDAC7 relative expression
HDAC9 relative expression
ns
****
siCT
siHDAC7
C
H1
H2
H3
H4
H4: K20ME2
H4: K16AC
H4: K8AC
H4: K5AC
H4: K20ME1
H4: K12AC
H4: K20ME3
H4: K20AC
H3.3: K27ME2
H3.1: K27ME2
H3.3: K36ME2
H3: K14AC
H3: K9ME2
H3: K23AC
** H3: K9ME1
** H3.3: K27ME1
H3.1: K27ME3
H3: K79ME1
H3.1: K36ME1
** H3.1: K27ME1
H3.1: K36ME2
H3.1: K36ME3
H3R2UN: K4ME1
H3.3: K36ME1
H3: K79ME2
H3.3: K36ME3
H3: K18AC
H3.3: K27ME3
H3: K9ME3
H3.3: K27AC
H3.3: K36AC
H3: K9AC
H3R2UN: Q5ME1
H3.1: K27AC
H3: K79AC
H3: R49ME2
H3.1: K36AC
H3R2UN: K4ME2
H3: K79ME3
H3: Q55ME1
H3R2UN: K4AC
H3: K18ME1
H3: K23ME1
H3R2UN: K4ME3
H3: Q19ME1
H3: R42ME2
H3: K56AC
H3: K64AC
H3: K56ME1
H3: K122AC
H3.3: K27M
H2A: K5AC
H2A: K9AC
H2A1: K15AC
H2A: K36AC
H2A1: K13AC
H2A3: K13AC
H2A3: K15AC
H2A1: K15UB
H1.4: K25ME1
H1.4: K25AC
H1.4: K25ME3
H1.4: K25ME2
D
Loss
Gain
H3K9UN
H3.1K27Me1
H3.3K27Me1
H3K9Me1
-log(p val)
Percent change (SiHDAC7/siCtrl)

Figure 3

A

RIME derived HDAC7 interactome

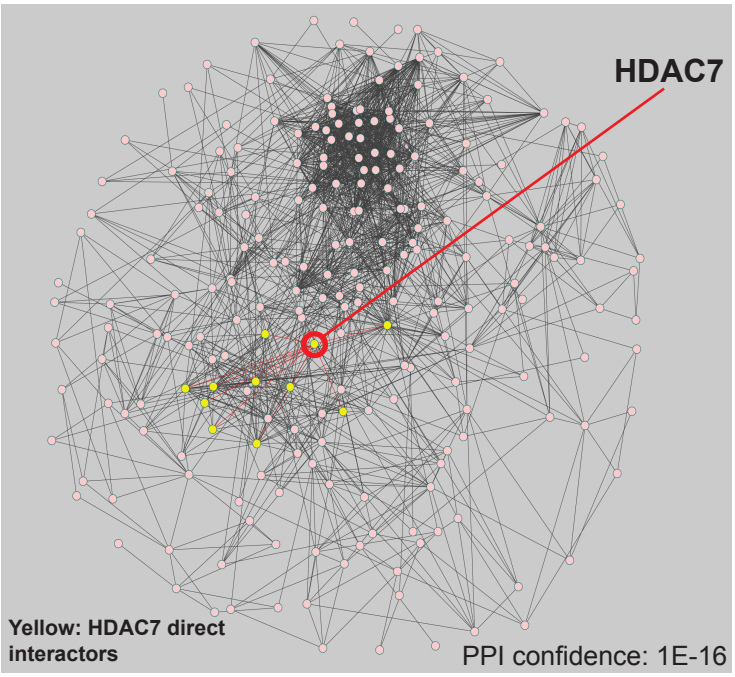

B

1st degree HDAC7 interactome

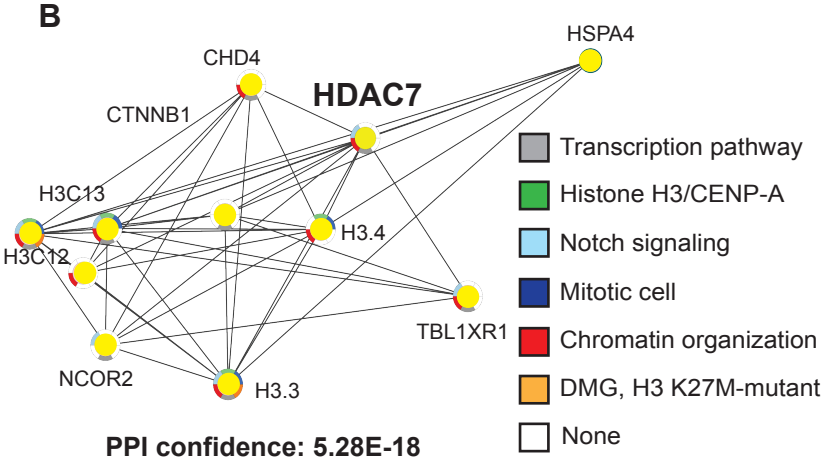

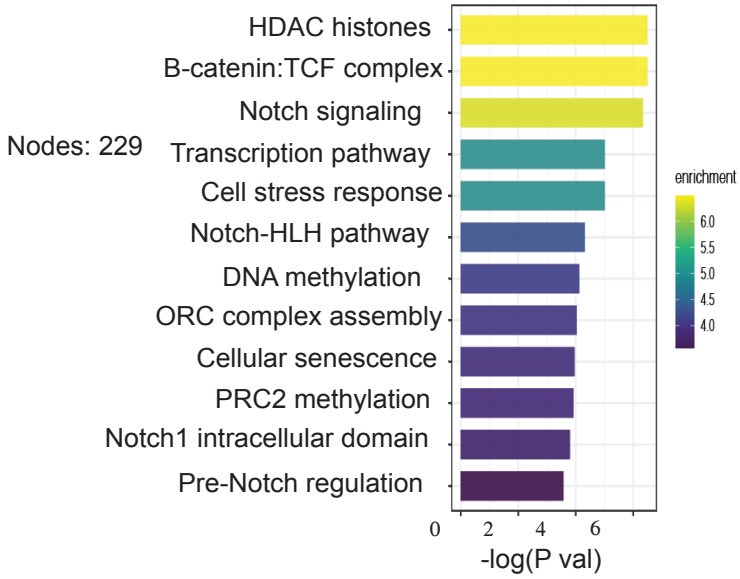

C

1st & 2nd degree HDAC7 interactome

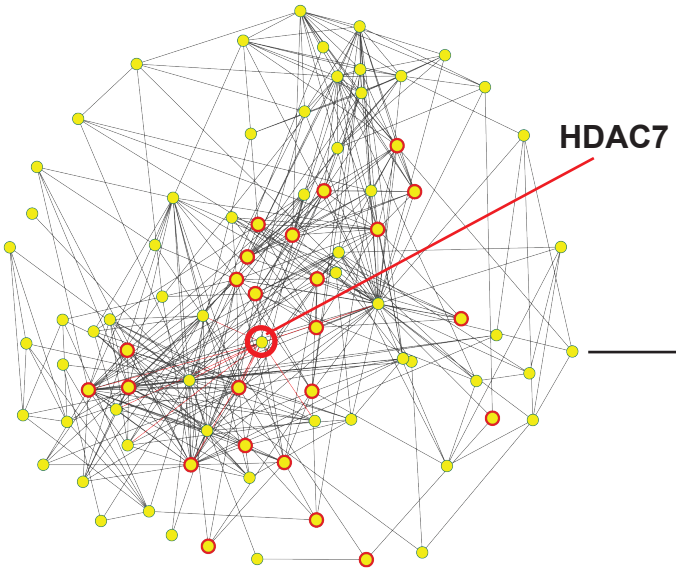

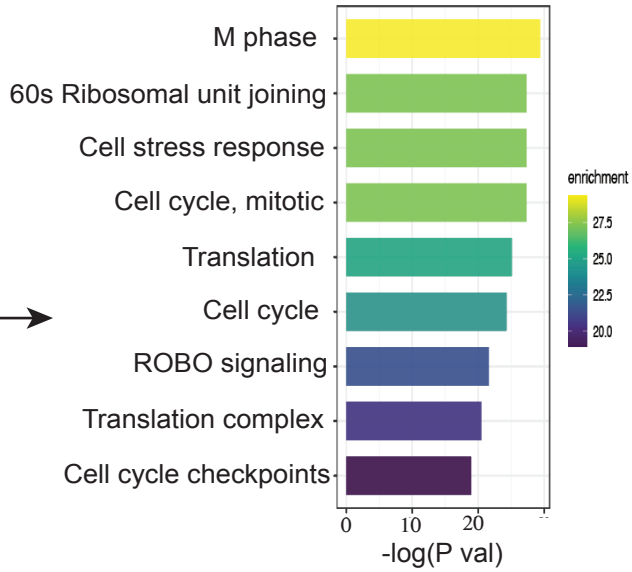

Figure 4

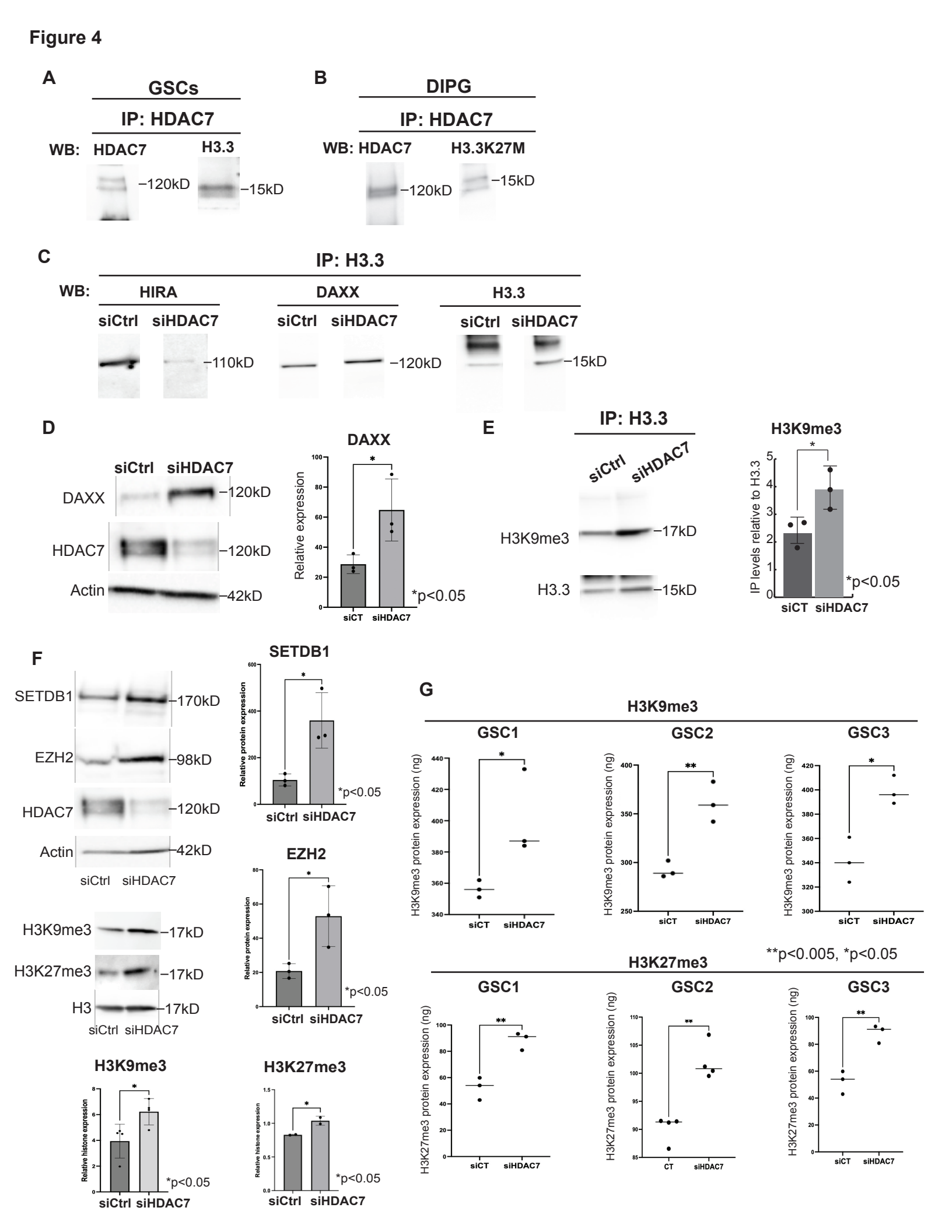
A
GSCs
IP: HDAC7
WB: HDAC7
H3.3
–120kD
–15kD
B
DIPG
IP: HDAC7
WB: HDAC7
H3.3K27M
–120kD
–15kD
C
IP: H3.3
WB:
HIRA
DAXX
H3.3
siCtrl siHDAC7
–110kD
–120kD
–15kD
D
siCtrl siHDAC7
DAXX
HDAC7
Actin
–120kD
–120kD
–42kD
DAXX
Relative expression
*p<0.05
siCT siHDAC7
E
IP: H3.3
siCtrl siHDAC7
H3K9me3
H3.3
–17kD
–15kD
H3K9me3
IP levels relative to H3.3
*p<0.05
siCT siHDAC7
F
SETDB1
EZH2
HDAC7
Actin
–170kD
–98kD
–120kD
–42kD
siCtrl siHDAC7
H3K9me3
H3K27me3
H3
–17kD
–17kD
–17kD
siCtrl siHDAC7
SETDB1
Relative protein expression
*p<0.05
siCtrl siHDAC7
EZH2
Relative protein expression
*p<0.05
siCtrl siHDAC7
H3K9me3
Relative histone expression
*p<0.05
siCtrl siHDAC7
H3K27me3
Relative histone expression
*p<0.05
siCtrl siHDAC7
G
H3K9me3
GSC1
GSC2
GSC3
H3K9me3 protein expression (ng)
siCT siHDAC7
**p<0.005, *p<0.05
H3K27me3
GSC1
GSC2
GSC3
H3K27me3 protein expression (ng)
siCT siHDAC7
CT siHDAC7

Figure 5

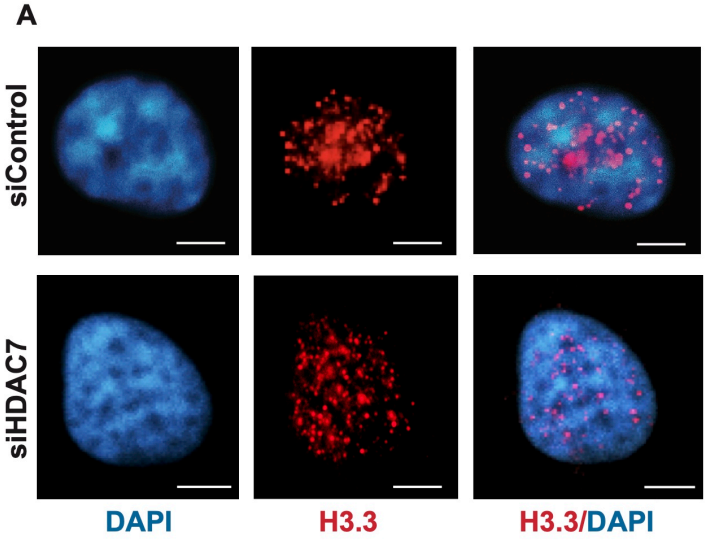
A
siControl
siHDAC7
DAPI
H3.3
H3.3/DAPI

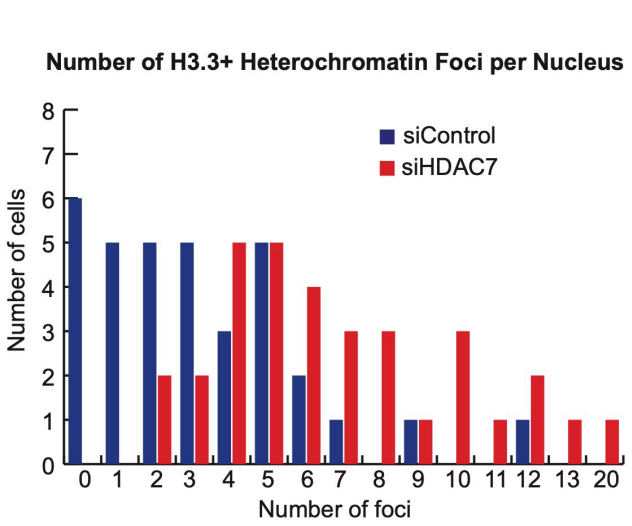
B
Number of H3.3+ Heterochromatin Foci per Nucleus
siControl
siHDAC7
Number of cells
0
1
2
3
4
5
6
7
8
0 1 2 3 4 5 6 7 8 9 10 11 12 13 20
Number of foci

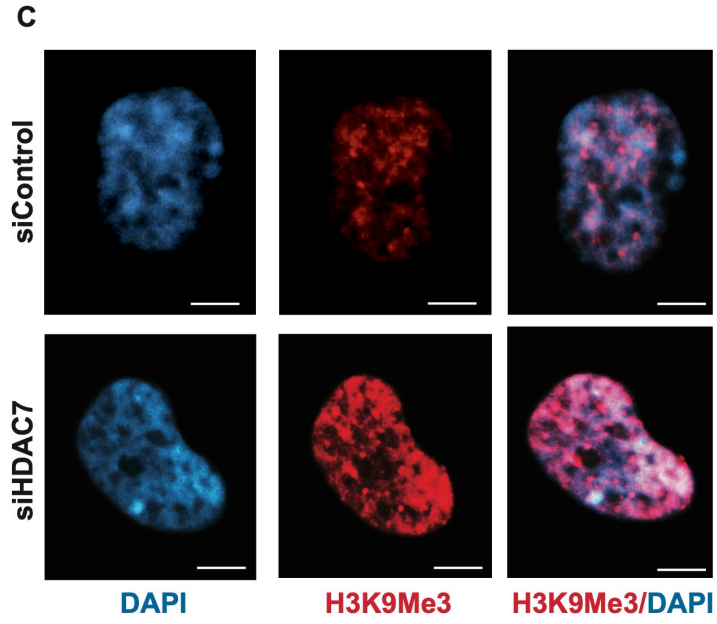
C
siControl
siHDAC7
DAPI
H3K9Me3
H3K9Me3/DAPI

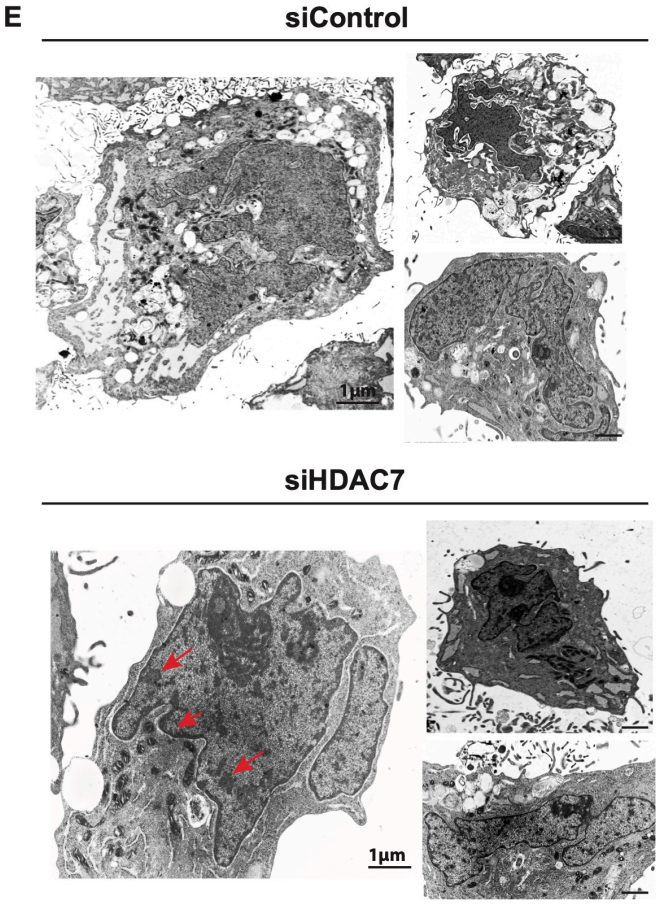
E
siControl
1µm
siHDAC7
1µm

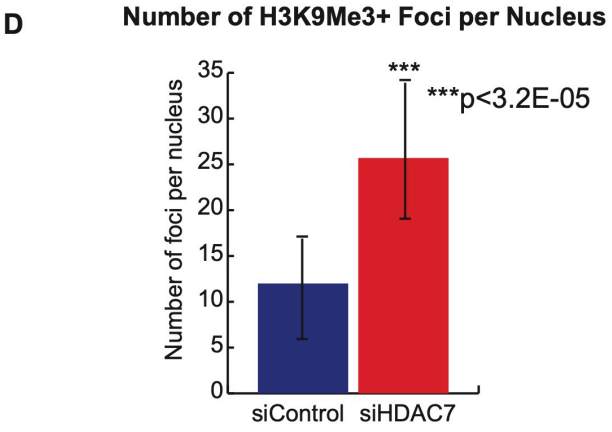
D
Number of H3K9Me3+ Foci per Nucleus
***
***p<3.2E-05
Number of foci per nucleus
0
5
10
15
20
25
30
35
siControl
siHDAC7

Figure 6

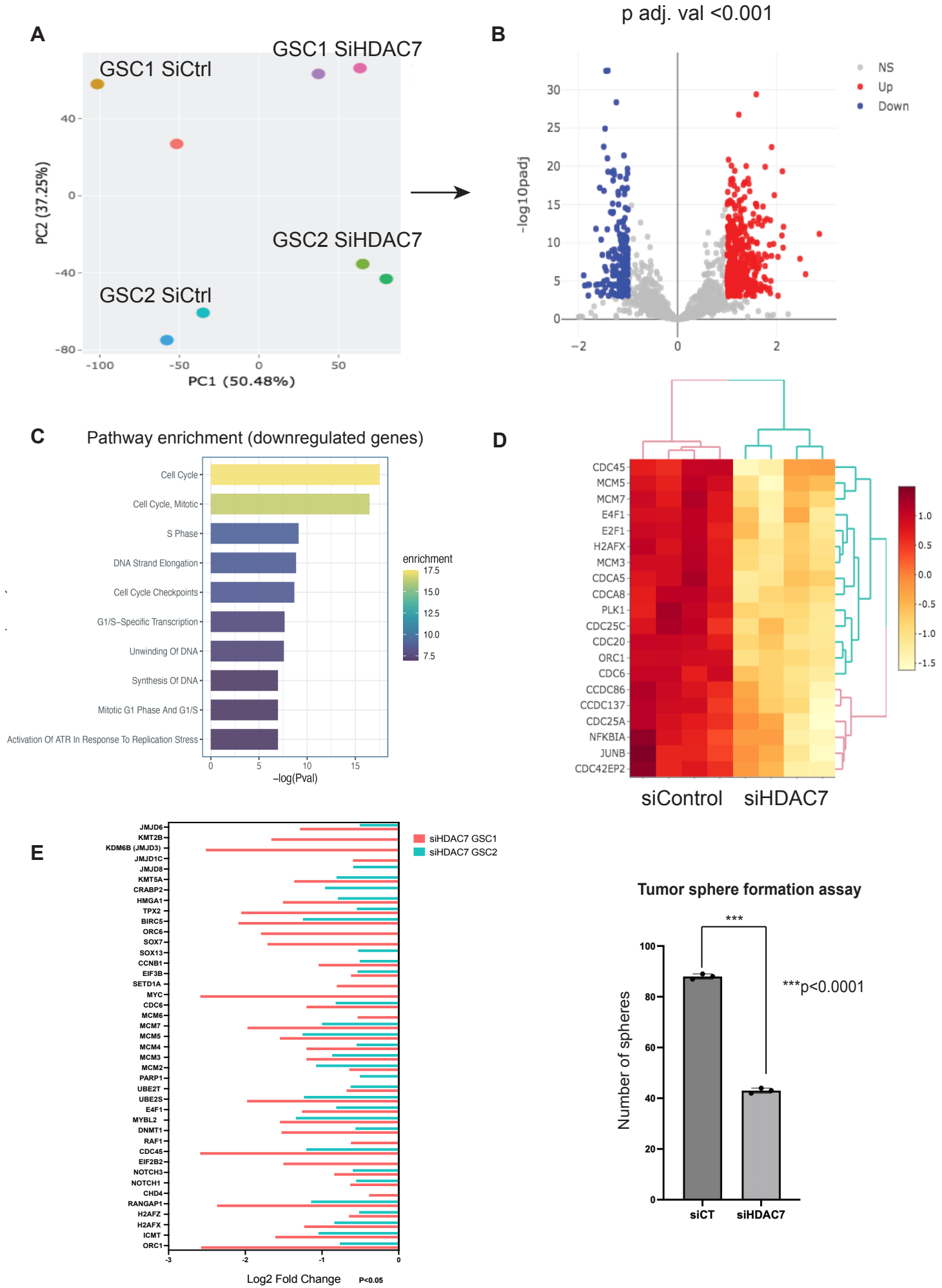
A
GSC1 SiCtrl
GSC1 SiHDAC7
GSC2 SiHDAC7
GSC2 SiCtrl
PC2 (37.25%)
PC1 (50.48%)
B
p adj. val <0.001
NS
Up
Down
-log10padj
C
Pathway enrichment (downregulated genes)
Cell Cycle
Cell Cycle, Mitotic
S Phase
DNA Strand Elongation
Cell Cycle Checkpoints
G1/S-Specific Transcription
Unwinding Of DNA
Synthesis Of DNA
Mitotic G1 Phase And G1/S
Activation Of ATR In Response To Replication Stress
enrichment
-log(Pval)
D
CDC45
MCM5
MCM7
E4F1
E2F1
H2AFX
MCM3
CDCA5
CDCA8
PLK1
CDC25C
CDC20
ORC1
CDC6
CCDC86
CCDC137
CDC25A
NFKBIA
JUNB
CDC42EP2
siControl
siHDAC7
E
siHDAC7 GSC1
siHDAC7 GSC2
Log2 Fold Change
P<0.05
Tumor sphere formation assay
***
***p<0.0001
Number of spheres
siCT
siHDAC7